RESEARCH ARTICLE
doi: 10.2306/scienceasia1513-1874.2026.059

ScienceAsia 52 (3): 2026: ID 2026059: **1–11**

Biomimetic lung cell membrane-coated nanoparticles for preferential targeting of nanoparticles to the lungs

Faprathan Pikwong[a,b], Jirayu Kangwan[c], Pongpeera Phum[c], Rapeepong Phaknonkul[c], Wattanased Jarisarapurin[a,b,d], Phornsawat Baipaywad[a,b], Sarawut Kumphune[a,b,*]

[a] Biomedical Engineering and Innovation Research Centre, Chiang Mai University — Mae Hia Campus, Chiang Mai 50100 Thailand
[b] Biomedical Engineering Institute, Chiang Mai University — Mae Hia Campus, Chiang Mai 50100 Thailand
[c] Science Classrooms in University-Affiliated School Project (SCiUS), Chiang Mai University Demonstration School, Chiang Mai 50200 Thailand
[d] Office of Research Administration, Chiang Mai University, Chiang Mai 50200 Thailand

[*]Corresponding author, e-mail: sarawut.kumphune@cmu.ac.th

Received 20 Mar 2026, Accepted 4 Jun 2026
Available online 30 Jun 2026

ABSTRACT: Acute lung injury (ALI) is a critical condition caused by rapid respiratory failure leading to an increase in fatality rates. Current treatment interventions largely provide support, as the drug delivery is severely limited by insufficient pulmonary localisation and systemic toxicity. Nanoparticles (NPs) have the potential for targeted delivery; however, their clinical application is complicated by rapid clearance from the mononuclear phagocyte system (MPS) and the possibility of immunogenicity. In this study, we developed a biomimetic drug delivery system consisting of lung cell membrane-coated mesoporous silica nanoparticles (LCM-MSNs). The cytotoxicity of LCM-MSNs in lung cells and the preferential cellular uptake in cardiomyocytes, lung cells, and vascular endothelial cells were evaluated. The immune evasion of LCM-MSNs was assessed using murine macrophages. Internalisation was determined by loading the rhodamine B (RhB)-fluorophore within LCM-MSNs and the PKH26-labelled cell membrane on the outer surface of LCM-MSNs, and observed by fluorescence imaging and the corrected total cell fluorescence measurements. The results demonstrated MSNs and LCM-MSNs maintained high biocompatibility at all concentrations. Fluorescent imaging revealed that while bare MSNs were internalised by all cell types, the LCM-MSNs demonstrated preferential uptake in lung cells. LCM-MSNs exhibited the strongest fluorescence signals in lung cells, while low uptake was observed in cardiomyocytes and vascular endothelial cells. Moreover, the LCM-MSNs showed less phagocytosis than MSNs. In conclusion, this study demonstrated the development of LCM-MSNs which represent nanomedicine technologies that improve preferential drug delivery to lung cells, potentially serving as an alternative approach for drug administration in ALI.

KEYWORDS: biomimetic nanomedicine, lung cell membrane, mesoporous silica nanoparticles, acute lung injury, homotypic targeting

INTRODUCTION

Acute lung injury (ALI) is a major global health problem, marked by a quick start of symptoms and higher death rates [1]. The causes of ALI are varied, usually divided into direct lung damage from factors such as viral or bacterial pneumonia, trauma, and toxic inhalation and indirect causes outside the lungs, such as sepsis, acute pancreatitis, and transfusion-related problems [2]. Lung injury relates to damage from epithelial and endothelial cells, as well as the extracellular matrix that supports these cells. This injury increases cellular protein expression and local inflammatory cells, inducing vascular permeability and the migration of inflammatory cells into the injured site. Although inflammatory cells are important for immune activation, they can also induce cellular damage [3]. Despite considerable therapeutic and research endeavours, the difficulty of achieving localised lung concentrations without inducing systemic toxicity continues to pose a significant obstacle. The absence of highly targeted delivery systems suggests that, except for mechanical ventilation, no definitive curative treatment for ALI is currently available in the clinical practice [4].

Nanoparticle-based drug delivery systems (DDSs) improve targeted drug delivery, reduce drug leakage, and provide prolonged controlled release [5]. Despite their advantages, nanoparticulate carriers from outside the body present significant physiological challenges. These carriers are rapidly removed by the mononuclear phagocyte system (MPS) through phagocytosis. Using nanoparticles (NPs) in large amounts could unintentionally damage lung epithelial cells, leading to an inflammatory immune response. This response then reduces their effectiveness in treating diseases [6].

Cell membrane carriers have become a key development in nanotechnology, offering significant advantages over traditional methods of delivering therapies [7]. Biologically derived cell membrane-coated NPs (CM-NPs) have attracted significant interest because of their potential for *in vivo* cell-like simulation and natural targeting abilities [8]. Moreover,

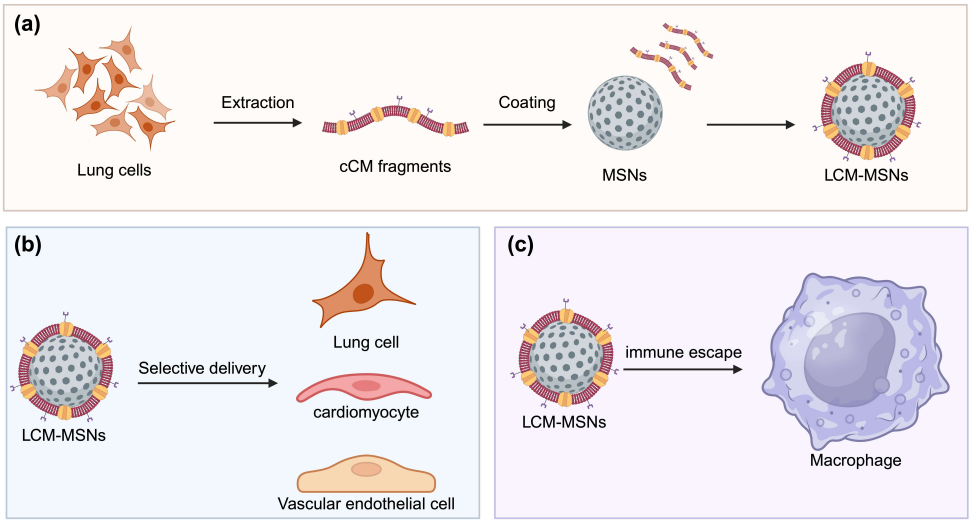

Fig. 1 Schematic of this study on LCM-MSNs. (a) Preparation; (b) Preferential delivery; (c) Immune evasion. (Created with BioRender.com).

the cell membrane coating mimics the surface characteristics of the source cell, allowing these NPs to evade immune system recognition, prolonging their circulation in the bloodstream and improving their capacity to target specific cells or tissues [9]. Therefore, to overcome the constraints of synthetic NPs, cell membrane-coated technologies have emerged as a more effective biomimetic strategy. CM-NPs represent a prospective advancement for the targeted and non-toxic delivery of medicines to the impaired lung environment. Our recently published work demonstrated for the first time that cardiac cell membrane-coated mesoporous silica nanoparticles (cCMCMSNs) provide a superior, targeted way to deliver drugs to the heart compared to standard, uncoated NPs [10]. This study focused on the preparation of lung cell membrane-coated mesoporous silica nanoparticles (LCM-MSNs) for pulmonary-preferential delivery and immune evasion to be an alternative biomimetic therapeutic delivery for recovery from lung injury (Fig. 1).

MATERIALS AND METHODS

Chemicals and reagents

Tetraethyl orthosilicate (TEOS) (98.0%), trimethyloctadecylammonium bromide (CTAB) (98%), 30% ammonia solution (NH_4OH), ethyl alcohol, PKH26 dye, and anti-pan cadherin antibody were purchased from Sigma-Aldrich (Milwaukee, WI, USA). Hydrochloric acid (HCl) was purchased from RCI Labscan Ltd., Bangkok, Thailand. The 3-(4,5-dimethyl-2-thiazol)-2,5-diphenyl-2H-tetrazolium bromide (MTT) was purchased from Ameresco (Solon, OH, USA). The horseradish peroxidase-conjugated secondary antibody was purchased from Merck (Darmstadt, Germany). In cell culture, reagents including Dulbecco's modified Eagle's medium (DMEM), DMEM/Nutrient Mixture F-12 (DMEM/F-12), foetal bovine serum, penicillin, streptomycin, and trypsin-EDTA were purchased from Gibco BRL, Life Technologies Inc., NY, USA).

Cell and cell culture

Adenocarcinoma from human alveolar basal epithelial cells (A549, CCL-185), adult human ventricular myocyte cell line (AC16, ATCC-CRL3568), human vascular endothelial cell line (EA.hy926, CRL-2922), and mouse macrophage cell line (RAW 264.7, TIB-71) were purchased from the American Type Cell Culture (ATCC, Manassas, VA, USA). Cells were cultured in the specific culture medium recommended by ATCC, supplemented with 10% (v/v) foetal bovine serum (FBS) and 100 units/ml of penicillin/streptomycin. The culturing condition was at 37 °C in a humidified atmosphere of 95% air and 5% carbon dioxide.

Preparation of mesoporous silica nanoparticles (MSNs)

The MSNs were synthesised using the modified Stöber method as previously reported [10, 11]. Briefly, CTAB was solubilised in a solution of ethanol and DI water, stirring at 750 rpm, 50 °C for 20 min. Subsequently, TEOS and 2 M NaOH were gradually incorporated into the solution while stirring for 2 h. After that, the reaction was cooled to room temperature until it attained 25 °C. The solution was centrifuged at 10,000 rpm for 10 min, and the pellet was subsequently washed twice with HCl-ethanol solution. The pellet was subsequently washed three times with DI water in ethanol concentrations of 50:20, 20:80, and 0:100. The NPs were finally acquired by a freeze-drying technique.

Lung cell membrane coating method

A549 cells were cultivated in a T-175 flask, then harvested at 80% confluence using trypsin-EDTA. The cells were rinsed twice with PBS and resuspended in 10 ml of hypotonic lysis buffer (50 mM Tris-HCl, pH 7.4, 10 mM magnesium sulphate, and one tablet of EDTA-free protease inhibitor). The cells were then mechanically disrupted by a rotor-stator probe homogeniser (D-160, DLAB Scientific, Beijing, China) at 6,000 rpm for 5 min. Subsequently, cell membranes were isolated by centrifugation at 100,000×g at 4 °C for 1 h and quantified using a Bradford assay. MSNs were coated with cell membranes in the ratio of 1:2. This ratio was chosen as the best formulation based on preliminary optimisation for comprehensive surface covering and colloidal stability. MSNs and cell membranes were exposed to sonication using a probe sonicator (UCD-950, Biobase, Jinan, China) at an energy input of 150 W with a 2-s pulse on and a 2-s pulse off for a total duration of 5 min in an ice bath. Subsequently, the solution was subjected to centrifugation at 10,000 rpm at 4 °C for 10 min to eliminate unbound cell membranes. Finally, LCM-MSNs were washed twice with and subsequently resuspended in PBS. LCM-MSNs were kept at 4 °C until use.

Physical characteristics of nanoparticles

NPs were characterised for size, polydispersity index (PDI), and zeta potential using a Zetasizer (Malvern, UK). To determine the morphology of NPs, particles were examined using a transmission electron microscope (TEM) (JEM-2010, JEOL, Tokyo, Japan) at 100 kV. The NPs were fixed with 2.5% glutaraldehyde for 30 min and subsequently dropped onto an EMS CF400-Cu-50 grid. After that, the grids were stained with a Uranyless solution for one min before examination.

Determination of cell membrane proteins by sodium dodecyl sulphate-polyacrylamide gel electrophoresis (SDS-PAGE) and Western blot

The proteins from extracted cells were determined by SDS-PAGE, including A549 lysate cells, MSNs, and LCM-MSNs. The samples were mixed with 2 × SDS sample buffer and boiled at 95 °C for 5 min. After that, the samples were run on 10% PAGE at 120 mV for 1 h 30 min. Then, the gel was stained with Coomassie brilliant blue R250 for 4 h and subsequently destained until the background of the gel was clear.

The protein marker of the cell membrane was determined using Western blot. Twenty micrograms of protein from each sample were loaded onto the gel. The gel that contains proteins was transferred onto a polyvinylidene fluoride (PVDF) membrane and blocked with 5% non-fat milk. The PVDF membrane was washed three times with TBST for 10 min each. After that, a pan-cadherin antibody as a primary antibody 1:1000 was added onto the membrane at 4 °C and incubated overnight. Then, the primary antibody solution was discarded and rinsed three times with TBST for 10 min each. Consequently, secondary antibody was added onto the membrane and incubated for 1 h at room temperature, followed by washing in TBST. The membrane that contains the band of protein profile was determined using the ChemiDoc™ Touch Imaging System (Bio-Rad Laboratories, Hercules, CA, USA).

Encapsulation and release

The investigation of encapsulation used rhodamine B (RhB) as described [10]. The MSNs were incubated with RhB for 24 h with shaking. The MSNs were then rinsed with PBS by centrifuging at 10,000 rpm for 10 min. The supernatant was collected to measure the encapsulation. The MSN pellet was resuspended with PBS and incubated with cell membranes for 30 min. The solution was subjected to the probe sonicator at 150 W with a 2-s pulse on and a 2-s pulse off for 5 min. The release time points over a 3-day period included 0, 1, 2, 6, 12, 24, 48, and 72 h. Both RhB-MSNs and RhB-LCM-MSNs were centrifuged at 10,000 rpm for 10 min at 4 °C. The supernatant was collected, and new PBS was added into the solution. The RhB was measured at 554 nm by a UV-vis spectrophotometer.

Cytotoxicity of NPs on lung cells

A549 cells were plated in a 96-well plate at a density of 10,000 cells/well and incubated for 24 h at 37 °C. The media were then discarded, and NPs were added for 24 h at 37 °C at the concentrations of 0.1, 1, 10, and 100 µg/ml, respectively. Subsequently, the NPs solution was removed, and a 0.5 mg/ml MTT solution was applied to the cells for 4 h at 37 °C. The MTT solution was ultimately eliminated. The formazan was extracted using DMSO. Cell viability was assessed using a microplate reader at 570 nm.

Nanoparticle staining

The MSNs were stained by the RhB dye, as previously reported [10]. Briefly, the MSNs were incubated with 0.04 mM RhB overnight. After incubation, MSNs were rinsed with DI water and centrifuged at 10,000 rpm for 10 min. The process was repeated until the supernatant was clear. The MSNs were suspended in PBS before determining the further examinations.

The PKH26 dye was employed to stain LCM-MSNs. One microlitre of PKH26 dye was incorporated into 250 µl of Diluent C provided with the kit. Then, the diluted PKH26 was combined with the diluted LCM-MSNs and incubated for 5 min. Then, a filtered FBS was utilised to terminate staining. The solution was centrifuged at 10,000 rpm for 10 min. This PKH26-LCM-MSN pellet was reconstituted in PBS and subjected to centrifugation at 10,000 rpm for 10 min. Finally, the PKH26-LCM-MSN pellet was reconstituted in DMEM before doing further investigations.

An *in vitro* preferential delivery of NPs

Three of the cell types, including A549, AC16, and EA.hy926 cells were seeded onto a 96-well plate at a density of 10,000 cells per well. When the cells had 80% confluence, the media were discarded, and 25 µg/ml RhB-MSNs and PKH26-LCM-MSNs were added and incubated for 4 h. The media were then discarded and cells were washed twice with PBS and preserved in a 4% paraformaldehyde solution for 20 min. Subsequently, the cells were permeabilised with 1% Triton X-100 for 10 min, then washed with PBS. The cells were stained with phalloidin and DAPI for 30 min and subsequently washed twice with PBS. The cellular uptake was observed using an EVOS M5000 fluorescence microscope (Thermo Fisher Scientific, Waltham, MA, USA) to capture fluorescent images of the cells. The quantification of internalisation was evaluated by ImageJ software using the calculation for corrected total cell fluorescence (CTCF) = integrated density − (area of selected cell × mean fluorescence of background readings), as previously described [12]. Mechanistically, by subtracting the environmental background noise, the CTCF value isolates and provides a precise quantitative representation of the true fluorescence intensity emitted exclusively by the internalised NPs within the defined cellular boundaries.

Immune evasion of NPs

To determine immune escape, RAW 264.7 cells were seeded on a 96-well plate at a density of 10,000 cells per well. To activate macrophages, bacterial lipopolysaccharide (LPS) from Sigma-Aldrich at 10 µg/ml was added and incubated for 24 h. Subsequently, the media were discarded and replaced with RhB-MSNs and LCM-MSNs at a concentration of 25 µg/ml for 4 h. Following incubation, the media were discarded, and the sample was washed twice with PBS. The cells were preserved in a 4% paraformaldehyde solution for 20 min, stained with DAPI for 30 min, and subsequently rinsed twice with PBS. The internalisation was observed using an EVOS M5000 fluorescence microscope to capture fluorescent images of the cells. The quantification of internalisation was evaluated using ImageJ software by determining the CTCF per cell and calculated as described above.

Statistical analysis

All experiments were performed in at least triplicate independent replicates ($n = 3$). The data was reported as the mean ± standard deviation (SD). The significance of all comparisons was determined using an unpaired t-test or ANOVA, followed by the Tukey–Kramer test. Statistical significance was indicated by a p-value that is less than 0.05.

RESULTS

Physical characteristics

The results demonstrated MSNs and LCM-MSNs could provide particle dimensions of 487.30 ± 7.02 nm and 511.90 ± 9.89 nm, respectively (Fig. 2a). There were significant differences when compared between sizes of NPs. The PDI of MSNs and LCM-MSNs was 0.33 ± 0.02 and 0.35 ± 0.05, which exhibited no significant statistics (Fig. 2b). The zeta potential of MSNs could show a charge of NPs as −21.80 ± 0.91 mV, while LCM-MSNs showed the charge of −34.14 ± 4.42 mV, exhibiting a significant difference (Fig. 2c). The result of SDS-PAGE showed a protein band of each sample lane, including A549 cell lysate, MSNs, A549 cell membrane, and LCM-MSNs (Fig. 2d). All samples exhibited the protein patterns except MSNs. The A549 showed similar protein pattern to that of the cell membrane and LCM-MSNs. Some bands of the proteins were absent due to purification by centrifugation. Noticeably, a band of pan-cadherin as a cell membrane marker from Western blot was exhibited in A549 lysate, the A549 cell membrane, and the LCM-MSNs (Fig. 2e).

Morphology of nanoparticles

The result demonstrated that both MSNs and LCM-MSNs mostly had a spherical shape (Fig. 3a,b). The TEM imaging in a dehydrated state complicates the visualisation of a distinct core-shell structure, as the fragile lipid bilayer often collapses onto the solid silica core under high vacuum; however, the morphological integrity and uniform spherical shape of the nanoparticles were distinctly maintained post-coating. Consequently, instead of depending exclusively on TEM, the successful membrane coating was conclusively validated through comprehensive orthogonal physicochemical and biological evidence, which encompassed the notable increase in hydrodynamic size, the alteration in zeta potential, and the preservation of functional membrane proteins.

Encapsulation and release profile

The MSNs and LCM-MSNs were determined for the encapsulation and release using RhB. The results demonstrated that RhB was encapsulated as 88.85 ± 2.10% and 87.33 ± 1.94% into MSNs and LCM-MSNs, respectively (Fig. 4a). After that, the NPs were evaluated for release profile, separating time points of 0, 1, 2, 6, 12, 24, 48, and 72 h, showing release of 3.60 ± 0.78%, 6.70 ± 1.15%, 8.63 ± 1.33%, 10.61 ± 1.38%, 25.39 ± 1.25%, 28.65 ± 2.00%, 30.86 ± 2.23%, and 37.02 ± 4.69% from RhB-MSNs, while LCM-MSNs showed the release of 5.57 ± 2.53%, 8.29 ± 2.26%, 10.41 ± 2.10%, 12.15 ± 2.22%, 15.33 ± 1.02%, 17.23 ± 1.17%, 20.51 ± 1.66%, and 22.80 ± 2.19%, respectively (Fig. 4b).

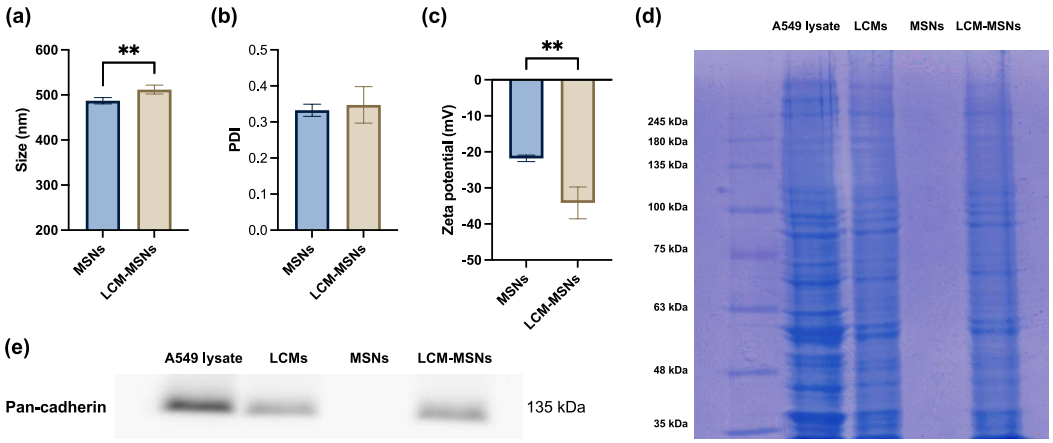

Fig. 2 Characteristics of NPs. (a) size; (b) PDI; (c) Zeta potential; (d) SDS-PAGE protein separation (Lane 1: A549 cell lysate, Lane 2: MSNs, Lane 3: A549 cell membrane, and Lane 4: LCM-MSNs); (e) The presence of lung cell membrane protein and pan-cadherin by Western blot. ** $p < 0.01$. Data are presented as mean ± SD ($n = 3$).

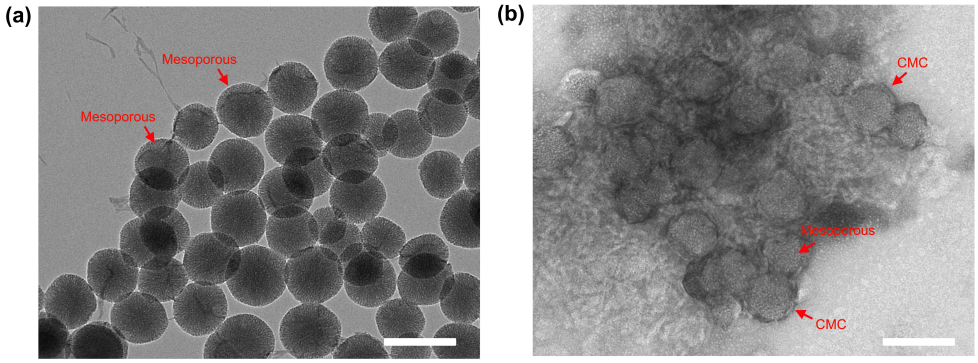

Fig. 3 Morphology of nanoparticles by TEM. (a) MSNs; (b) LCM-MSNs. Scale bar = 100 nm. CMC = Cell membrane coating.

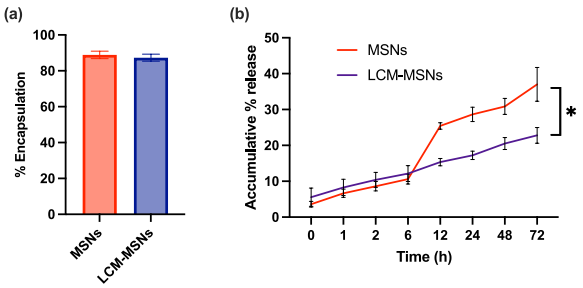

Fig. 4 The RhB encapsulation and release profiles of MSNs and LCM-MSNs. (a) Encapsulation efficiency of RhB; (b) cumulative percentage of release of RhB over a 72-h period, * $p < 0.05$. Data are presented as mean ± SD ($n = 3$).

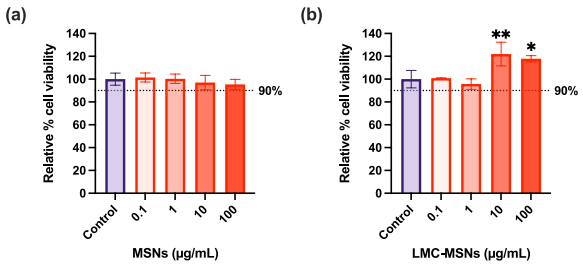

Fig. 5 Cytotoxicity of nanoparticles on lung cells. (a) Cytotoxicity of MSNs; (b) Cytotoxicity of LCM-MSNs, * $p < 0.05$ and ** $p < 0.01$. Data are presented as mean ± SD ($n = 6$).

Cytotoxicity of nanoparticles

The cytotoxicity of MSNs at the concentrations 0.1 to 100 μg/ml was 101.40 ± 3.94%, 100.30 ± 3.94%, 96.99 ± 6.33%, and 95.34 ± 4.49%, respectively, while LCM-MSNs at the same concentration range showed cytotoxicity of 100.90 ± 0.24%, 95.71 ± 4.60%, 122.00 ± 10.35%, and 117.90 ± 2.76%, respectively (Fig. 5a, b). In MSNs, there were no significant differences in toxicity when compared to control (100.00 ± 5.30%). In contrast, LCM-MSNs at 10 and 100 μg/ml were significantly different when compared to the control (100.00 ± 7.67%).

Preferential internalisation of nanoparticles

The fluorescent imaging demonstrated the selectivity of the LCM-MSNs in lung cells (A549), cardiomyocytes (AC16), and vascular endothelial cells (EA.hy926), respectively. The results showed that RhB-MSNs were internalised by three cell types, as demonstrated by the detection of red fluorescence signals within the cells. The fluorescence signal of PKH26-LCM-MSNs was highest in A549 cells (Fig. 6a). However, the fluorescence signal in AC16 and EA.hy926 exhibited minimal uptake following treatment with PKH26-LCM-MSNs (Fig. 6b, c). The quantitative evaluation of the CTCF/cell for the internalisation of RhB-MSN in three cell types was 993.40 ± 173.00 AU, 6,317.00 ± 2,077.00 AU, and 5,234.00 ± 2,610.00 AU, respectively. However, the uptake of RhB-LCM-MSNs in each of these cases was 25,535.00 ± 6,066.00 AU, 15,470.00 ± 3,029.00 AU, and 8,159.00 ± 3,265.00 AU, respectively (Fig. 6d).

Immune evasion

To evaluate the immune escape, the results demonstrated the uptake of NPs from macrophages (RAW 264.7 cells) that were induced by LPS to be M1 macrophages before assessing immune evasion. A strong red fluorescence signal of MSNs was shown. In contrast, macrophages treated with LCM-MSNs displayed a noticeably reduced red fluorescence signal (Fig. 7a). The quantitative data showed that the cellular uptake of MSNs and LCM-MSNs was 9,582.00 ± 3,098.00 AU and 3,962.00 ± 567.80 AU, respectively (Fig. 7b). The LCM-MSNs were significantly lower than bare MSNs.

DISCUSSION

In this study, we selected the A549 cell line to extract lung cell membranes because this cell line is recognised and used *in vitro* as a representative model for lung epithelial cells that provide the preserved surface antigenic characteristics of the lung cells for targeted delivery, rather than primary human alveolar cells. Moreover, the A549 cell line is a proliferating cell line that can be simply cultured and expanded to extract membranes on a large scale.

The complete coating of the lung cell membrane onto MSNs was confirmed by an increase in hydrodynamic size, approximately 24 nm from the biological lipid bilayer [13]. This hydrodynamic size of the LCM-MSNs is primarily evaluated based on the Brownian motion of particles in a medium, which increases apparent hydrodynamic size [14]. Therefore, this result conforms with the TEM image, indicating that the dehydrated form of the NPs under vacuum could show a smaller structural shape. Moreover, the consistent PDI indicated that the coating process could not result in significant particle aggregation and showed a homogeneous distribution of the membrane throughout the MSNs [15]. The increased negative charge of LCM-MSNs is indicative of the electrical properties of the A549 cell membrane. This enhanced electronegativity, which is less than −20 mV, is an indicator of effective coating and improves the colloidal stability of the NPs through electrostatic repulsion [16]. In the result from SDS-PAGE, the lack of protein bands in the MSN lane indicates the inorganic composition of the core. The similarity in protein profiles among the A549 lysate, the cell membrane, and the LCM-MSNs indicates that the crucial membrane proteins were successfully coated to the NPs [17]. The slight absence of certain bands in the cell membrane and LCM-MSNs, relative to the whole-cell lysate, is likely due to the purification processes by centrifugation that exclude cytoplasmic and nuclear proteins [9, 18]. To confirm the presence of the cell membrane protein, the identification of pan-cadherin, a known cell membrane marker, in the A549 lysate, cell membrane, and LCM-MSN samples provides strong evidence for membrane orientation and retention [19]. However, pan-cadherin was used mostly as a reliable structural biomarker to confirm the integrity of the cell membrane coating process, rather than as a specific pathogenic target for ALI.

To confirm the cell membrane coating method, the NPs were determined by TEM. The bare MSNs presented a spherical shape. Following the membrane-coating process, the LCM-MSNs also had a round shape. Although the resolution of the TEM imaging used in this study could not provide a clear visualisation of the internal mesopores or core-shell structure, the effective functionalisation of the MSNs is confirmed by biological characterisations. Moreover, this MSN from the same protocol of MSN preparation was evaluated for pore-specific surface area using the Brunauer-Emmett-Teller (BET) theory. It showed a pore size around 18.81 ± 11.25 nm which confirmed that the inside remained porous [10]. An approximately 24 nm increase in hydrodynamic size, a significant electronegative shift in zeta potential, and the retention of membrane-specific proteins collectively confirm the successful coating of the lung cell membrane onto the MSN core. Moreover, the resemblance to a lipid bilayer coating might suggest improved structural integrity and heightened stability, which are essential for maintaining the functionality of NPs during their interactions with biological systems [10]. Although LCM-MSNs seem densely aggregated in the TEM image, this clustering is primarily an artefact resulting from the dehydration process during TEM sample preparation, wherein the drying of the lipid bilayer induces significant interparticle interactions. In an aquatic environment, as corroborated by the PDI findings, they stay adequately disseminated.

Both MSNs and LCM-MSNs showed high cargo-loading capabilities, making them potentially useful for therapeutic delivery. This high loading efficiency

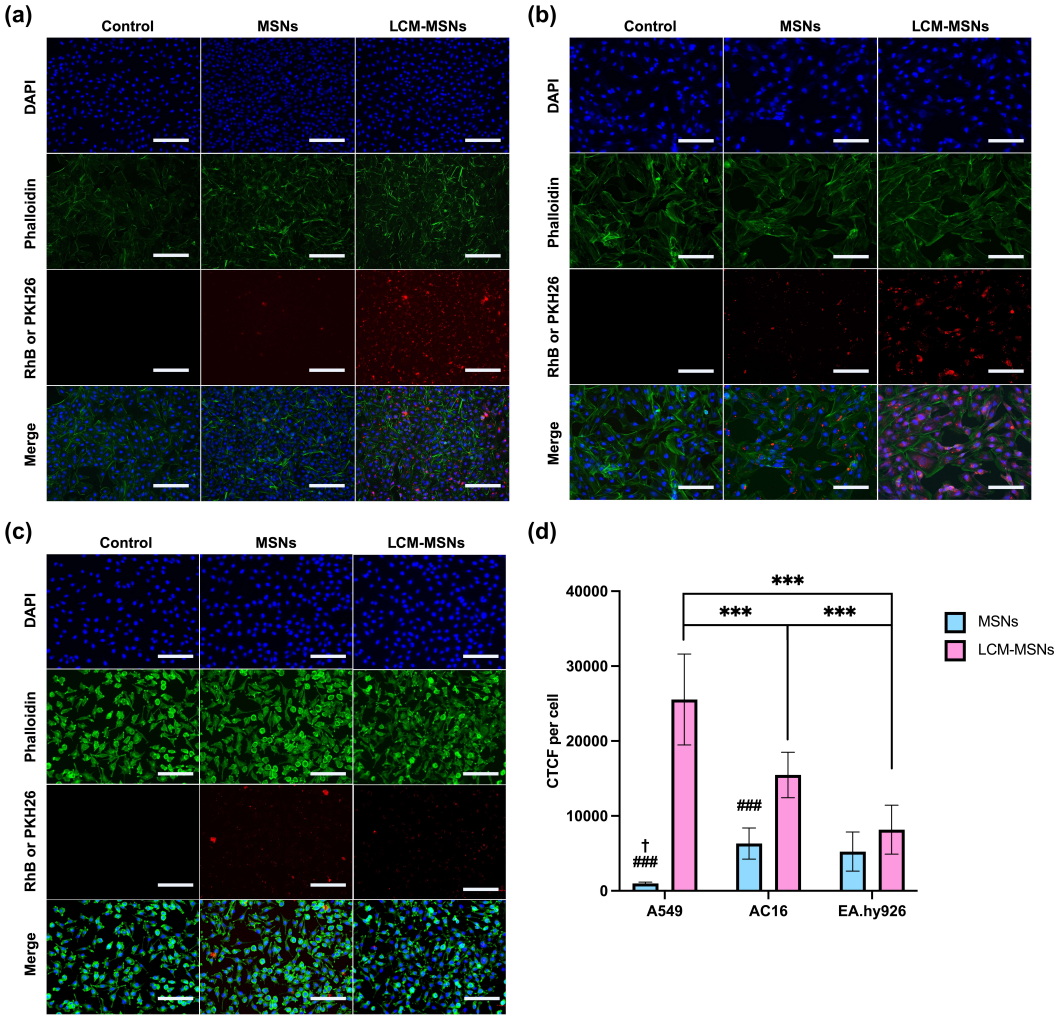

Fig. 6 Preferential internalisation of NPs. (a) Lung cell (A549); (b) Cardiomyocyte (AC16); (c) Vascular endothelial cell (EA.hy926); (d) CTCF)/cell of NP internalisation. *** $p < 0.001$ vs. LCM-MSNs group; ### $p < 0.001$ MSNs vs. LCM-MSNs in each group; † $p < 0.05$ vs. MSNs group. Scale bar = 150 µm. Data are presented as mean ± SD ($n = 6$).

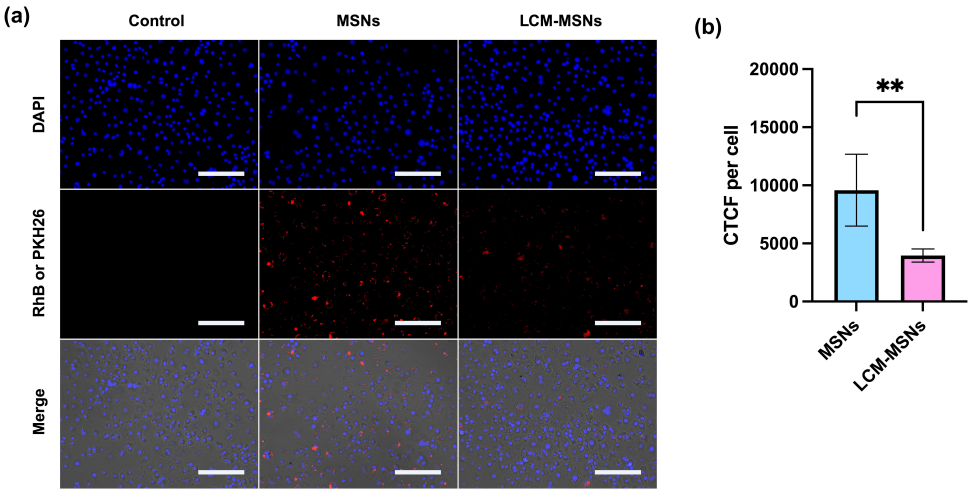

Fig. 7 Immune evasion of NPs. (a) Internalisation of NPs in macrophages; (b) CTCF)/cell of NP internalisation. ** $p < 0.01$. Scale bar = 150 µm. Data are presented as mean ± SD ($n = 6$).

of RhB is attributed to the large surface area and the mesoporous volume. The porous structure could promote strong electrostatic interactions between the MSN surface and the RhB, providing high stability and efficient encapsulation [20, 21]. In traditional drug delivery platforms, such as liposomes or polymeric NPs, there are often challenges with low encapsulation efficiency for hydrophilic molecules that are able to generally load less than 60% due to limited internal volumes [22]. The observed high encapsulation efficiency is crucial for delivering a therapeutic concentration of the cargo at the target site, consequently optimising efficacy and minimising systemic toxicity. Furthermore, the release profiles indicated that RhB exhibited a considerably accelerated release rate from uncoated MSNs relative to the LCM-MSN. The initial burst release from the bare MSNs might be associated with the uncontrolled circulation of RhB via the open mesoporous structure, allowing rapid solvent access to the encapsulated molecules. Conversely, the cell membrane coating on LCM-MSNs seems to act as a significant physical and diffusional barrier [23]. The lipid bilayer and associated membrane proteins might impede the external diffusion of RhB, resulting in a more controlled and extended release pattern [24]. In contrast to the previous study reported by Jakaria et al [25], which employed A549 cell membrane-coated dextran NPs (A549 NPs) to encapsulate curcumin LCM-MSNs exhibited an encapsulation efficiency of 87.33% for RhB. LCM-MSNs exhibited a highly regulated and sustained release profile, with a 22.80% release within 72 h, in contrast to A549 NPs, which exhibited an early burst release of 15–30% within 24 h. This suggests that the MSN mesoporous structure and the biological lipid bilayer work in collaboration to establish a diffusion barrier that is highly effective. Therefore, this sustained release profile is highly relevant for the clinical conditions of ALI from a therapeutic perspective. The controlling release could minimise the risk of local dose-dependent adverse effects, which is particularly crucial when delivering potent pharmacological agents to injured lung tissues. The prolonged and slow release of therapeutic agents over 72 h might be beneficial with the crucial duration of the acute inflammatory phase in ALI, potentially offering a continuous therapeutic opportunity without requiring multiple doses. Suggesting that the LCM-MSN system could offer a prolonged therapeutic duration, thus reduce the frequency of administration and improve patient compliance in long-term drug delivery applications. However, this release demonstrated a regulated release over 72 h in PBS solution that is useful for a baseline release mechanism. Moreover, it does not represent the complex physiological microenvironment of the lungs, particularly altered pH conditions associated with ALI. Therefore, future investigation is needed to evaluate the rate of release in clinical conditions that mimic inflammation to enhance understanding of the efficacy of LCM-MSNs in practical therapeutic applications.

This study investigated the cytotoxicity of bare MSNs and LCM-MSNs across a wide concentration range (0.1 to 100 µg/ml). The results indicated that MSNs and LCM-MSNs had a high level of cell viability (higher than 90%) and minimal cytotoxicity. This result showed that the MSNs had excellent natural biocompatibility and that the biomimetic membrane coating could maintain this excellent biocompatibility without adverse effects [26]. The cell viability of approximately 122% following treatment with high concentrations of LCM-MSNs could be attributed to the biological properties of the biomimetic coating and the intrinsic mechanism of the MTT assay, which evaluates mitochondrial activity. The lung cell membrane is abundant in homologous lipids, proteins and trace signalling chemicals [27]. These factors could serve as nutritional supplements or activate homologous receptor-mediated signalling pathways after interaction with cultured A549 cells. This interaction can temporarily enhance cellular metabolic activity and mitochondrial function or stimulate minor cellular growth, resulting in an amplified formazan signal compared to the untreated control [28]. Significantly, the bare MSNs did not generate this associated rise in absorbance, suggesting that the observed effect is not an experimental artefact resulting from particle light scattering but rather a distinct biological reaction to the cell membrane coating [29]. Furthermore, the LCM coating serves as a stealth layer, reducing the direct interface between the surface of core NPs and the cell membrane, therefore preventing the physical membrane disruption that may occur with uncoated inorganic NPs [9].

To evaluate the biological identity and targeting delivery of these designed NPs, we performed comparative fluorescence imaging across three unique cell lines: A549 (lung cells), AC16 (cardiomyocytes), and EA.hy926 (vascular endothelial cells). Our results presented strong evidence that the LCM coating fundamentally modifies the cellular internalisation of the MSNs, converting them from a non-specific to a highly preferential delivery system. The most significant result was the substantial fluorescence signal detected exclusively in A549 cells treated with LCM-MSNs. A quantitative analysis of CTCF revealed that uptake in A549 cells was almost threefold more than in vascular cells and greatly exceeded the uptake of bare MSNs in the same cell line. The high improvements in the uptake of LCM-MSNs relative to their uncoated MSNs suggest that the lung cell membrane provides a targeting efficiency. It is suggested that this cell-type-specific targeting is facilitated by the preservation of native surface proteins on the lung cell membranes, which interact more efficiently with lung cells than with non-target cardiovascular cell types. This mechanism is called 'homotypic targeting', which provides a self-recognition process wherein LCM-MSNs preferentially

adhere to and are internalised by cells via ligand-receptor interactions [30]. Similar to the report by Jakaria et al [25] that suggested the uptake of A549 cell membrane-coated dextran NPs could provide extremely high internalisation in lung adenocarcinoma cells for enhancing pulmonary transcytosis compared to other types of cell membrane-coated NPs. While previous studies focused on the translocation of NPs via the pulmonary epithelium for systemic delivery, our investigation specifically confirms the specific homotypic targeting properties of LCM-MSNs in a multi-cell-type study setting, demonstrating substantially enhanced preferential internalisation in A549 lung cells relative to non-target cells (cardiomyocytes and vascular endothelial cells). However, direct comparison of the internalisation efficiency of our LCM-MSNs with the A549 NPs reported by Jakaria et al [25] is unfeasible due to the utilisation of different analytical methodologies and fluorophores (ImageJ-based CTCF of RhB vs plate reader-based quantification of curcumin). The significantly enhanced absorption of LCM-MSNs by lung cells indicates that the drug carrier has potential for targeted drug delivery in pulmonary applications. This selectivity could improve the therapeutic efficacy of lung treatments due to its reduced off-target effects.

Avoiding rapid clearance by the mononuclear phagocyte system is crucial for successful targeted drug delivery [10]. We evaluated the immune-evasive characteristics by an *in vitro* macrophage uptake assay. The results clearly demonstrated that the LCM-MSNs effectively escaped phagocytosis. The improved stealth property is primarily attributed to the biomimetic cloaking presented by the cell membrane [31]. MSNs are generally at risk of opsonisation, the rapid adsorption of serum proteins upon entering a circulation, which exposes them for rapid identification and elimination by the mononuclear phagocyte system (MPS) [32]. By coating the MSNs with cell membranes, the resulting LCM-MSNs receive a natural lipid bilayer and essential endogenous surface proteins. This membrane coating reduces non-specific protein binding and promotes active immunological tolerance, typically mediated by specific surface markers that effectively suppress macrophage phagocytosis [17]. Thus, the significant decrease in macrophage uptake indicates that LCM-MSNs have higher potential for immune evasion, which could result in prolonged circulation in the bloodstream and increased accumulation at the target therapeutic site in future *in vivo* applications. Nonetheless, although the decreased uptake by *in vitro* macrophage models suggests potential stealth characteristics, it offers insufficient evidence for total systemic immune evasion. Subsequent in vivo immunological investigations will be necessary to thoroughly assess the actual immune clearance and circulation half-life of these NPs.

This study successfully synthesised a biomimetic nanoplatform by camouflaging MSNs with native lung cell membranes (LCM-MSNs). This biologically generated strategy offers two functional advantages to the NPs: preferential uptake by lung cells and reduced internalisation by macrophages. The results demonstrated that the LCM-MSNs exhibit sustained and controlled drug release, while ensuring high biocompatibility and low toxicity in lung cells, comparable to the bare MSNs. In addition, these persuasive findings highlight the novel potential of the drug delivery. This delivery technology, specifically designed to overcome significant physiological challenges, effectively addresses issues like “off-target” effects and immune system clearance. Therefore, this LCM-MSN, by specifically targeting the alveolar epithelium, has the potential to treat ALI by effectively delivering encapsulated anti-inflammatory or reparative medicines to the damage site while reducing systemic exposure.

A crucial limitation of the present study is that it relied exclusively on an *in vitro* model. While the research successfully establishes a proof-of-concept for utilising lung cell membranes to augment the functionality of NP surfaces, thereby facilitating improved preferential tissue delivery, the present findings necessitate further exploration of their physiological implications. Therefore, further study should determine the targeting efficacy in *in vivo* models, potentially using small animal imaging to track the biodistribution of LCM-MSNs. Furthermore, to adapt these drug delivery systems into clinical applications, further study should encapsulate therapeutic drugs within the LCM-MSNs and investigate their protective effects on lung cells under pathological conditions. In this study, the cellular internalisation determined by widefield fluorescence microscopy primarily demonstrates strong cellular association with the cells. However, to confirm intracellular internalisation, utilising confocal microscopy with Z-stack imaging will be required to precisely map the intracellular trafficking and distinguish complete internalisation from strong membrane adherence. These studies will provide crucial functional data relevant to human diseases while also offering significant molecular insights that could inform targeted ALI therapies. Ultimately, establishing the long-term safety profile of LCM-MSN targeted delivery in both small and large animal models is a critical prerequisite before initiating clinical trials. Furthermore, to adapt these drug delivery systems into clinical applications, further study should encapsulate therapeutic drugs within the LCM-MSNs and investigate their protective effects on lung cells under pathological conditions, for example, using LPS-induced ALI *in vivo* models [33].

CONCLUSION

In conclusion, this study reveals an advancement in biomimetic drug delivery systems utilising LCM-MSNs for preferential lung delivery. The biomimetic coating conferred substantial functional benefits, such as high encapsulation efficiency, controllable release capabil-

ity, enhanced biocompatibility, and facilitated specific homotypic targeting of lung cells, leading to greatly enhanced cellular internalisation relative to non-target cells. Moreover, the cell membrane camouflage provided the NPs with highly effective immune-evasive properties, substantially reducing macrophage phagocytosis. Thus, this approach provides a highly promising and applicable alternative strategy for surface modification in nanomedicine. These biomimetic nanovesicles offer several potential benefits for treating the physiological problems associated with ALI. They could improve the effectiveness of localised treatments while also reducing the risk of systemic toxicity.

Acknowledgements: This study was supported by Chiang Mai University (CMU) for SK, and CMU Presidential Scholarship 2023 for FP. This project is funded by Science Classrooms in University-Affiliated School Project (SCiUS), CMU Demonstration School, the National Research Council of Thailand (NRCT): High-Potential Research Team Grant Program Contract no. N42A650870 for SK and the CMU Proactive Researcher Program, CMU (Grant number EX010163) for WJ.

REFERENCES

1. Zhang J, Jiang S, Jiang J, Liu Y (2025) Global research landscape on nanotechnology in acute lung injury: Aa bibliometric analysis. *Front Digit Health* **7**, 1472753.
2. Liu H, Dong J, Xu C, Ni Y, Ye Z, Sun Z, Fan H, Chen Y (2025) Acute lung injury: pathogenesis and treatment. *J Transl Med* **23**, 926.
3. Fan W, Gui B, Zhou X, Li L, Chen H (2024) A narrative review on lung injury: mechanisms, biomarkers, and monitoring. *Crit Care* **28**, 352.
4. Zhang S, Zhao X, Xue Y, Wang X, Chen XL (2024) Advances in nanomaterial-targeted treatment of acute lung injury after burns. *J Nanobiotechnology* **22**, 342.
5. Zhang S, Zhang X, Gao H, Zhang X, Sun L, Huang Y, Zhang J, Ding B (2024) Cell membrane-coated biomimetic nanoparticles in cancer treatment. *Pharmaceutics* **16**, 531.
6. Zheng X, Zhang T, Huang T, Zhou Y, Gao J (2022) Cell-derived membrane biomimetic nanocarriers for targeted therapy of pulmonary disease. *Int J Pharm* **620**, 121757.
7. Cai D, Liu L, Han C, Ma X, Qian J, Zhou J, Zhu W (2019) Cancer cell membrane-coated mesoporous silica loaded with superparamagnetic ferroferric oxide and paclitaxel for the combination of chemo/magnetocaloric therapy on MDA-MB-231 cells. *Sci Rep* **9**, 14475.
8. Zhao Y, Zhu X, Hu L, Hao F, Ji X, Hu X, Luo M, Zheng L, et al (2025) Macrophage membrane-coated polydopamine nanomedicine for treating acute lung injury through modulation of neutrophil extracellular traps and M2 macrophage polarization. *Mater Today Bio* **32**, 101708.
9. Desai N, Tambe V, Pofali P, Vora LK (2024) Cell membrane-coated nanoparticles: A new frontier in immunomodulation. *Adv NanoBiomed Res* **4**, 2400012.
10. Pikwong F, Kamsarn J, Jarisarapurin W, Baipaywad P, Park H, Kumphune S (2025) Cardiac cell membrane-coated nanoparticles as a potential targeted delivery system for cardiac therapy. *Biomimetics (Basel)* **10**, 141.
11. Rahmani S, Durand J-O, Charnay C, Lichon L, Férid M, Garcia M, Gary-Bobo M (2017) Synthesis of mesoporous silica nanoparticles and nanorods: Application to doxorubicin delivery. *Solid State Sci* **68**, 25–31.
12. Jakic B, Buszko M, Cappellano G, Wick G (2017) Elevated sodium leads to the increased expression of HSP60 and induces apoptosis in HUVECs. *PLoS One* **12**, e0179383.
13. Chugh V, Vijaya Krishna K, Pandit A (2021) Cell membrane-coated mimics: A methodological approach for fabrication, characterization for therapeutic applications, and challenges for clinical translation. *ACS Nano* **15**, 17080–17123.
14. Jia Z, Li J, Gao L, Yang D, Kanaev A (2023) Dynamic light scattering: A powerful tool for *in situ* nanoparticle sizing. *Colloids Interfaces* **7**, 15.
15. Danaei M, Dehghankhold M, Ataei S, Hasanzadeh Davarani F, Javanmard R, Dokhani A, Khorasani S, Mozafari MR (2018) Impact of particle size and polydispersity index on the clinical applications of lipidic nanocarrier systems. *Pharmaceutics* **10**, 57.
16. Rasmussen MK, Pedersen JN, Marie R (2020) Size and surface charge characterization of nanoparticles with a salt gradient. *Nat Commun* **11**, 2337.
17. Liu L, Bai X, Martikainen M-V, Kårlund A, Roponen M, Xu W, Hu G, Tasciotti E, et al (2021) Cell membrane coating integrity affects the internalization mechanism of biomimetic nanoparticles. *Nat Commun* **12**, 5726.
18. Ma X, Chen Z, Chen W, Chen Z, Meng X (2024) Exosome subpopulations: The isolation and the functions in diseases. *Gene* **893**, 147905.
19. Ibata N, Terentjev EM (2022) Nucleation of cadherin clusters on cell-cell interfaces. *Sci Rep* **12**, 18485.
20. Igaz N, Bélteky P, Kovács D, Papp C, Rónavári A, Szabó D, Gácser A, Kónya Z, et al (2022) Functionalized mesoporous silica nanoparticles for drug-delivery to multidrug-resistant cancer cells. *Int J Nanomedicine* **17**, 3079–3096.
21. Baig MM, Yousuf MA, Alsafari IA, Ali M, Agboola PO, Shakir I, Haider S, Warsi MF (2021) New mesostructured origami silica matrix: A nano-platform for highly retentive and pH-controlled delivery system. *J Taibah Univ Sci* **15**, 133–144.
22. Li Q, Li X, Zhao C (2020) Strategies to obtain encapsulation and controlled release of small hydrophilic molecules. *Front Bioeng Biotechnol* **8**, 437.
23. Gao W, Zhang L (2015) Engineering red-blood-cell-membrane-coated nanoparticles for broad biomedical applications. *AIChE J* **61**, 738–746.
24. Ashley CE, Carnes EC, Phillips GK, Padilla D, Durfee PN, Brown PA, Hanna TN, Liu J, et al (2011) The targeted delivery of multicomponent cargos to cancer cells by nanoporous particle-supported lipid bilayers. *Nat Mater* **10**, 389–397.
25. Jakaria MG, Sorkhdini P, Yang D, Zhou Y, Meenach SA (2022) Lung cell membrane-coated nanoparticles capable of enhanced internalization and translocation in pulmonary epithelial cells. *Int J Pharm* **613**, 121418.
26. Shen H, Ouyang Y, Zhang L, Li J, Wang S (2024) Blood cell membrane-coated nanomaterials as a versatile biomimetic nanoplatform for antitumor applications. *Nanomaterials* **14**, 1757.
27. Ghasemi M, Turnbull T, Sebastian S, Kempson I (2021)

The MTT assay: Utility, limitations, pitfalls, and interpretation in bulk and single-cell analysis. *Int J Mol Sci* **22**, 12827.
28. Yaman S, Chintapula U, Rodriguez E, Ramachandramoorthy H, Nguyen KT (2020) Cell-mediated and cell membrane-coated nanoparticles for drug delivery and cancer therapy. *Cancer Drug Resist* **3**, 879–911.
29. Kroll AV, Fang RH, Zhang L (2017) Biointerfacing and applications of cell membrane-coated nanoparticles. *Bioconjug Chem* **28**, 23–32.
30. Zhang X, Ren J, Wang J, Li S, Zou Q, Gao N (2018) Receptor-mediated endocytosis generates nanomechanical force reflective of ligand identity and cellular property. *J Cell Physiol* **233**, 5908–5919.
31. Liu Y, Luo J, Chen X, Liu W, Chen T (2019) Cell membrane coating technology: A promising strategy for biomedical applications. *Nanomicro Lett* **11**, 100.
32. Fam SY, Chee CF, Yong CY, Ho KL, Mariatulqabtiah AR, Tan WS (2020) Stealth coating of nanoparticles in drug-delivery systems. *Nanomaterials* **10**, 787.
33. Cen F, Wei Y, Zhang X, Liu H, Chen G (2025) AS-1 attenuates the inflammatory response by targeting AKT and MAPK in LPS-activated acute lung injury models. *ScienceAsia* **51**, 2025048.